Climate-related vegetation characteristics derived from Moderate Resolution Imaging Spectroradiometer (MODIS) leaf area index and normalized difference vegetation index

Ping Zhang and Bruce Anderson
Department of Geography, Boston University, Boston, Massachusetts, USA

Mathew Barlow
Atmospheric and Oceanic Diagnostics, AER Inc, Lexington, Massachusetts, USA

Bin Tan and Ranga B. Myneni
Department of Geography, Boston University, Boston, Massachusetts, USA

Received 1 March 2004; revised 2 July 2004; accepted 20 July 2004; published 19 October 2004.

[1] MODIS-based leaf area index (LAI) and normalized difference vegetation index (NDVI) are used to examine detailed information regarding actual growing season and total annual production for various regions. Overall, MODIS LAI has larger variability and demonstrates more information regarding the evolution and structure of the seasonal vegetation characteristics. In contrast, the NDVI saturates around 0.7 and tends to overestimate the growing season in regions where it is already long. Next, a climatic impact index (CII) is derived to provide additional information regarding the potential sensitivity of vegetation to changes in climatic variables by accounting for the length of growing season. By normalizing the growth rate to the biome-average growth rate, this index can identify fractional loss of annual production, as opposed to the absolute loss which may be strongly weighted by the overall growth rate for different ecosystems. Our index provides a quantitative framework for assessing the importance of the length of the growing season in determining climatic vulnerability. In the last part of the paper, we use the long time series AVHRR products as a substitute for the MODIS products and test the temporal characteristics of the CII. Major drought events are well-captured by the CII, suggesting potential use as a monitoring and evaluation tool. Furthermore, the strong positive correlation between the CII and the vegetation condition index (VCI) suggests that the CII can quantitatively identify the effects of climatic variability upon vegetation activity. *INDEX TERMS:* 1620 Global Change: Climate dynamics (3309); 1640 Global Change: Remote sensing; 1812 Hydrology: Drought; 3322 Meteorology and Atmospheric Dynamics: Land/atmosphere interactions; *KEYWORDS:* MODIS, leaf area index, growing season, climate variability, vegetation monitoring

Citation: Zhang, P., B. Anderson, M. Barlow, B. Tan, and R. B. Myneni (2004), Climate-related vegetation characteristics derived from Moderate Resolution Imaging Spectroradiometer (MODIS) leaf area index and normalized difference vegetation index, *J. Geophys. Res.*, *109*, D20105, doi:10.1029/2004JD004720.

1. Introduction

[2] Global vegetation is strongly affected by drought, especially when it is persistent. To compare droughts spatially and temporally, a standardized index of drought is needed, but disagreements about defining drought have so far made this difficult.

[3] Drought indices have previously been derived from precipitation, expressed as the duration or intensity of droughts [*Wilhite and Glantz*, 1985]. On the basis of only precipitation, these indices work well only for specific regions, however the definition of droughts is highly variable globally [*Heim*, 2002]. *Palmer* [1965] combined temperature and precipitation to develop a set of indices that can measure both the short- and long-term moisture conditions. The Palmer indices are widely used in the United States [*Hu and Willson*, 2000]. However, they are limited to semiarid and arid climates, where local precipitation is the primary source of moisture [*Guttman*, 1991; *Guttman et al.*, 1992; *Hayes et al*, 1999]. *McKee et al.* [1993] developed the standardized precipitation index (SPI) that can identify drought or wet events at a given temporal scale for any station that has historic rainfall data. The SPI compares droughts in different regions better than the Palmer indices do [*Guttman*, 1997]. However, the SPI is based on knowledge of the climatology of the study region, and one assumption of the SPI is that all locations have the same

0148-0227/04/2004JD004720$09.00

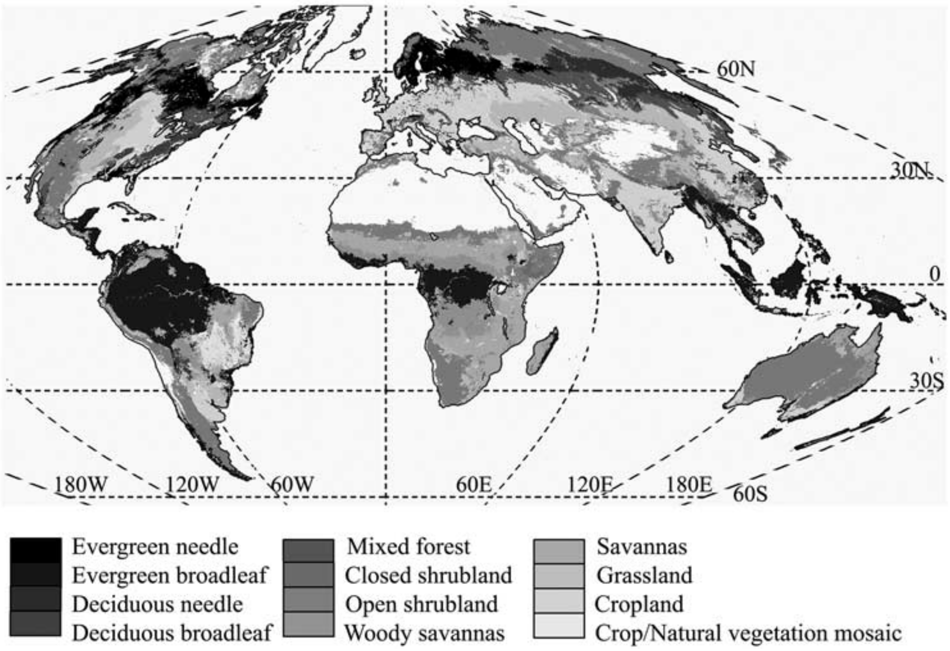

Figure 1. Global MODIS IGBP land cover map (only with major classes). See color version of this figure in the HTML.

frequency of severe and extreme drought [*Hayes et al.*, 1999].

[4] Another type of drought index, which examines the impact of drought upon vegetation directly, is computed from the normalized difference vegetation index (NDVI) data provided by the advanced very high resolution radiometer (AVHRR) satellite [*Kogan*, 1990, 1995; *Peters et al.*, 2002]. The vegetation condition index (VCI) can detect drought density, duration, and effect on vegetation [*Kogan*, 1990, 1995]. It is widely applied in real-time drought monitoring over the world, and is a potential universal index. *Peters et al.* [2002] developed a standardized vegetation index (SVI) for drought monitoring. Their results demonstrate that the SVI can provide a near-real-time indicator of vegetation conditions. One limitation of these NDVI-based drought indices is that NDVI is usually saturated at densely vegetated regions [*Carlson and Ripley*, 1997; *Paltridge and Barber*, 1988], which will decrease the quality of the indices during high-growth periods.

[5] In addition to NDVI, the leaf area index (LAI) is a potential source for generating a universal drought index. The LAI is defined as the one-sided green-leaf area per unit ground area in broadleaf canopies and as the projected needleleaf area in coniferous canopies [*Myneni et al.*, 2002]. The LAI is a valuable criterion of vegetation production and is used as a key parameter in most ecosystem productivity models and global models of climate, hydrology, biogeochemistry and ecology [*Sellers et al.*, 1997]. Furthermore, by definition, the LAI represents the growth mass itself and is directly related to energy and mass exchanges.

[6] Presently, both the NDVI and LAI have a strong legacy using AVHRR measurements. Unfortunately, the AVHRR data is not ideally suited for vegetation monitoring applications because of the lack of precise calibration, poor quality of geometric registration, and difficulties in cloud screening [e.g., *Goward et al.*, 1991; *Sellers et al.*, 1994]. Unlike the AVHRR, the radiometric and geometric properties of the Moderate Resolution Imaging Spectroradiometer (MODIS) provide a substantially improved basis for such studies [*Justice et al.*, 1998; *Running et al.*, 1994; *Zhang et al.*, 2003]. Given the high temporal and spatial resolution of the MODIS NDVI and LAI, and their improved atmospheric correction and cloud screening, they are qualified for analyzing vegetation activity such as seasonal and annual growth.

[7] In this paper, we quantify the climatological characteristics of the MODIS LAI and NDVI data sets. From these, we develop a climatic impact index (CII), which can provide additional information regarding the sensitivity of certain regions to changes in climatic variables, such as droughts. Data for this research is introduced in section 2. The characteristic and evaluation of the NDVI and LAI are presented in section 3, followed by some comparisons of their results. The CII is discussed in section 4. The temporal characteristics of the CII are shown in section 5 using the long time series of AVHRR data, together with some discussion and concluding remarks.

2. Data

2.1. MODIS IGBP Land Cover Map

[8] The MODIS land cover classification product identifies 17 classes of land cover in the International Geosphere-Biosphere Programme (IGBP) global vegetation classification scheme [*Friedl et al.*, 2002]. This scheme includes 11 classes of natural vegetation, 3 classes of developed land, permanent snow or ice, barren or sparsely vegetated land, and water (Figure 1). The latest version of

the IGBP land cover map at 16-km resolution is used to help identify how climatic variations affect biomes.

2.2. MODIS LAI

[9] The retrieval technique of the MODIS LAI algorithm is as follows. For each land pixel, given red and near-infrared reflectance values, along with the Sun and sensor angles and a biome-type designation, the MODIS LAI algorithm uses a model-generated lookup table to identify likely LAI values corresponding to the input parameters given above. This radiative transfer–based lookup is done for a suite of canopy structures and soil patterns that represent a range of expected natural conditions for the given biome type. The mean value of the LAI values found within this uncertainty range is taken as the final LAI retrieval value. In certain situations, if the algorithm fails to localize a solution either because of biome misclassification/mixtures, high uncertainties in input reflectance data or algorithm limitations, a backup algorithm is utilized to produce LAI values based upon the empirical relation between NDVI and LAI [*Myneni et al.*, 1997].

[10] For this analysis, the latest version of MODIS global LAI from February 2000 through December 2003 at 16-km resolution was taken to characterize the global vegetation activity, such as seasonal and annual production. This monthly data set was generated using Collection 4 MODIS LAI/FPAR 8-day products which are distributed to the public from the Earth Resources Observation System (EROS) Data Center Distributed Active Archive Center (EDC DAAC). The 8-day products also provide quality control variables for each LAI value that indicate its reliability. To generate the monthly global data set, only the LAIs with reliable quality are composited over each month and then averaged to coarser spatial resolution. The monthly global products at 1- and 4-km resolution with sinusoidal (SIN) projection are available at Boston University (W. Yang et al., Analysis of global MODIS leaf area index and fraction absorbed PAR time series data from February 2000 to December 2003, submitted to *Journal Geophysical Research*, 2004) (hereinafter referred to as Yang et al., submitted manuscript, 2004). In this paper, the 4-km data are averaged over four by four pixels to generate the 16-km MODIS global LAI. For convenience, we will refer to this product as simply "LAI"; other LAI products derived from different data sources will be identified by their relevant data source. This will also be the case for the MODIS NDVI data (see below).

2.3. MODIS NDVI

[11] The MODIS NDVI is a normalized ratio of the near-infrared (841–876 nm) and red (620–670 nm) reflectance. MODIS NDVI is currently being produced at 16-day intervals at various spatial resolutions [*Huete et al.*, 1994, 1997]. The products are generated from the level 2 daily surface reflectance products which are corrected for molecular scattering, ozone absorption, and aerosols [*Vermote et al.*, 2002]. The 1-km NDVI is aggregated from 250- and 500-m NDVI products.

[12] In this study, we used global MODIS NDVI from March 2000 through September 2003 at 2-km resolution (75% are the latest version). The MODIS LAI and NDVI are reported at different spatial and temporal resolutions. To make these two products comparable, the NDVI is aggregated into 16-km resolution sets and then reprojected on the sinusoidal (SIN) projection. The difference and correlation between NDVI and LAI are discussed in section 3.

2.4. Climate Data

[13] We used the Climate Prediction Center (CPC) merged analysis of precipitation (CMAP) to identify global patterns of ecologically significant water surplus and deficit. The CMAP data are monthly precipitation (mm/d), from 1979 to 2002 at 2.5° spatial resolution. The data are produced by merging gauge observations, precipitation estimates from five different satellite-based algorithms, and output from numerical model predictions [*Xie and Arkin*, 1997]. For this work, the CMAP will be used to generate long time series of SPI and demonstrate the relationship between rainfall and vegetation activity in general.

2.5. AVHRR LAI and NDVI

[14] AVHRR LAI is used as a substitute for the MODIS LAI to examine the temporal characteristics of vegetation activity for longer time periods. The AVHRR LAI is derived from AVHRR NDVI using radiative transfer models [*Myneni et al.*, 1997]. As mentioned, it is the AVHRR NDVI that is used to generate the Vegetation Condition Index [*Kogan*, 1990 and 1995]. The relationship between CII and VCI is discussed in section 5.

[15] Two sets of AVHRR data, Pathfinder and GIMMS, are used in this paper. The AVHRR Pathfinder NDVI and LAI are monthly data from 1982 to 2000 at 16-km resolution, produced by Boston University. The Pathfinder data are reported at Goode's projection, which is different from MODIS data. To make these two products comparable, the Pathfinder data are reprojected on the sinusoidal (SIN) projection. AVHRR Global Inventory Modeling and Mapping Studies (GIMMS) NDVI is monthly data from 1981 to 2002 at 0.25° resolution, produced by NASA GIMMS group. Several important improvements are made in the following steps: maximum value composition bimonthly; correction for residual sensor degradation and sensor intercalibration differences [*Vermote and Kaufman*, 1995; *Los*, 1998]; correction of stratospheric aerosols [*Vermote et al.*, 1997]; correction of cloud cover; and correction for solar zenith angle and viewing angle effects [*Rosborough et al.*, 1994].

3. Characteristic of MODIS LAI and NDVI

[16] The principal mode of vegetation variability is generally associated with intra-annual seasonality. The seasonality of leaf mass or vegetation production can be quantitatively described as a function of time, such as symmetrical sine curve [*Waggoner*, 1974] or Gaussian distribution [*Lieth*, 1970]. To examine the seasonality in the remote sensing products, let $X(p, m, y)$ be the vegetation index (LAI or NDVI) of pixel p at month m year y. The multiyear average vegetation index of month m is defined as

$$\overline{X}(p,m) = \frac{1}{N_y} \sum_{y=2000}^{2003} X(p,m,y), \qquad (1)$$

where N_y is the number of years (N_y = 3 or 4). Because vegetation growth varies greatly between different ecosys-

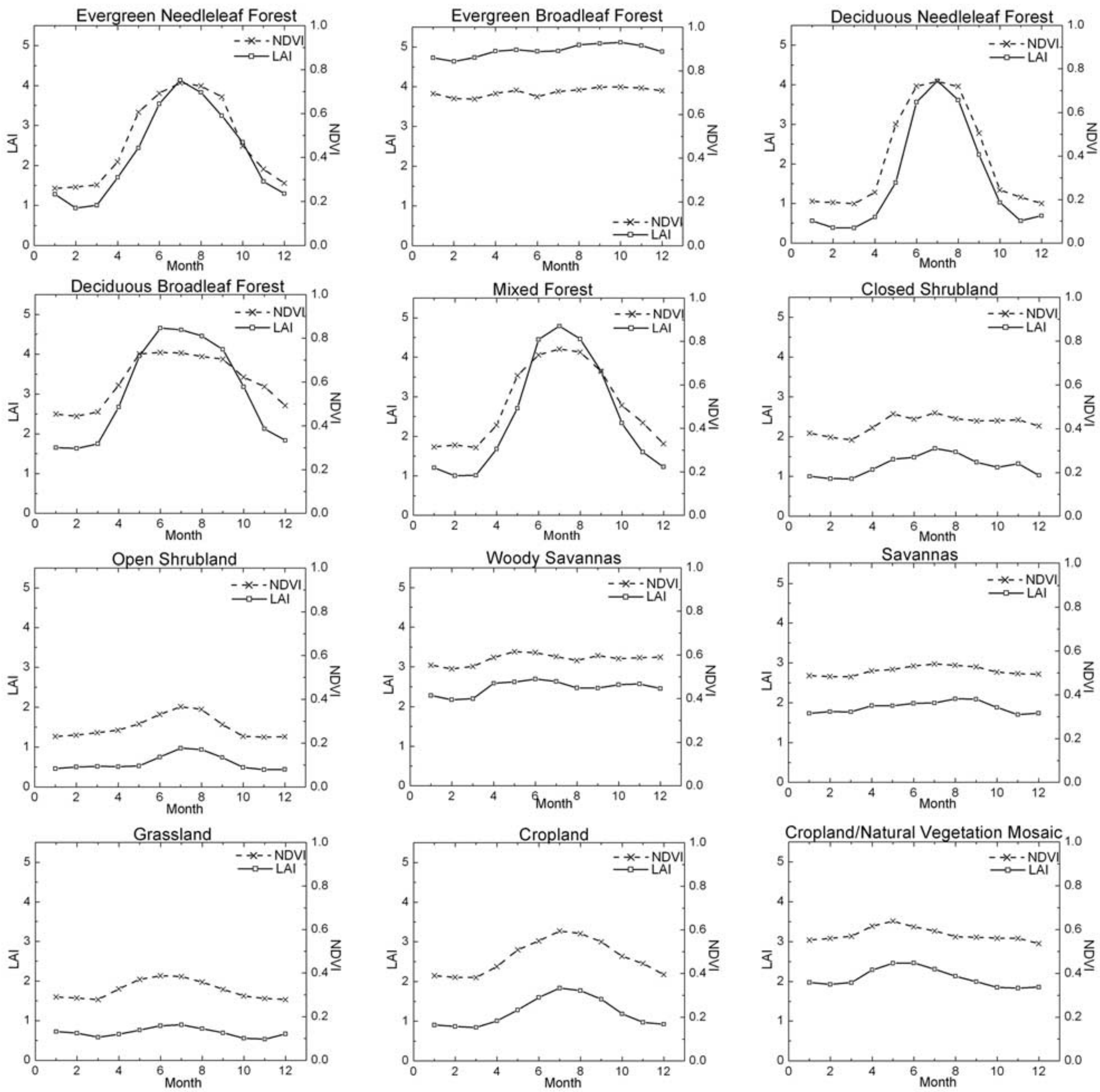

Figure 2. Climatological monthly MODIS vegetation index for major land cover classes defined by International Geosphere Biosphere Programme (left y axis shows LAI, and right y axis shows NDVI). The x axis represents the calendar month. For Southern Hemisphere, high-latitude dates (>23°S) are shifted by 6 months to account for the shift in hemispheric seasons.

tems, spatial aggregation in land cover classes is necessary. For a given land cover type l, let N_l be the total number of the pixels for that land cover type, then the biome-specific, spatial-average climatological index $X(l, m)$ is calculated as

$$X(l,m) = \frac{1}{N_l} \sum_p \overline{X}(p,m). \qquad (2)$$

[17] Since the purpose of this study is to find an index that can demonstrate vegetation sensitivity to climate variability, we are not interested in some land cover classes, such as permanent wetlands, and developed lands. These classes are excluded in the following analysis. Furthermore, to alleviate the opposite seasonality of the two hemispheres, grid points in the southern high latitudes (>23°S) are shifted in time by 6 months. The climatological MODIS LAI and NDVI for the major land cover classes are shown in Figure 2. Most classes have a significant growing peak during the summer, with the exception of evergreen broadleaf forest; its vegetation index remains high (approximately 5.0 for LAI and 0.7 for NDVI) for the whole year. Other forests have Gaussian distributions centered in hemispheric summer with a maximum LAI/NDVI around 5/0.7 and a minimum

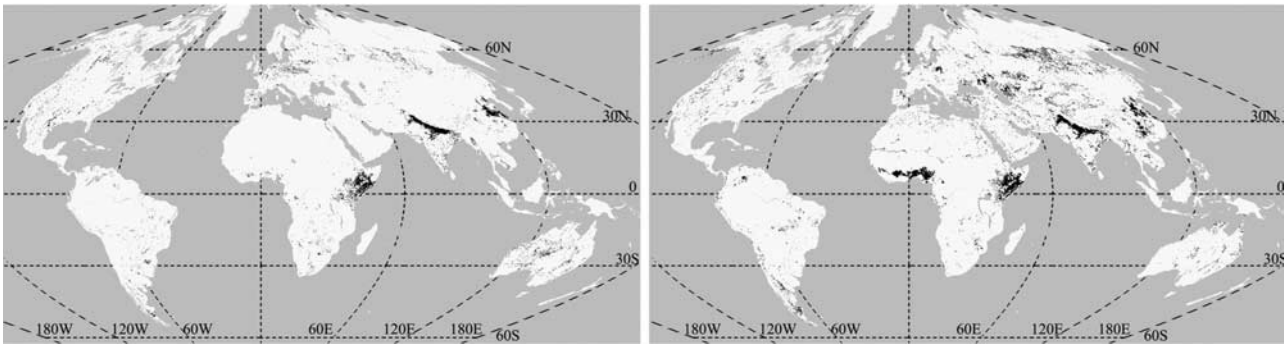

Figure 3. Pixels with more than one growing season generated from 16-km MODIS vegetation index. (left) MODIS LAI and (right) MODIS NDVI.

LAI/NDVI around 1/0.3. The decrease of evergreen needleleaf forest in winter is not surprising when considering the snow cover, which hides the actual vegetation growth [e.g., *Tian et al.*, 2004]. The maximum LAI/NDVI in arid and semiarid ecosystems (shrublands, savannas, grasslands) is about 2/0.4, much less than the forests. In sum, the MODIS LAI/NDVI can quantify spatial differences between productivity of ecosystems as well as seasonal variations in each ecosystem. However, the variations in NDVI are much smaller than LAI, especially over high-growth regions when the NDVI saturates around 0.7. In particular, the NDVI in forest regions tends to plateau during the summer, while the LAI shows more variability.

[18] AVHRR NDVI has been applied to examine the growing season of different ecosystems already, using specific NDVI thresholds [e.g., *White et al.*, 1997] or backward looking moving averages [*Reed et al.*, 1994]. In this paper, we use threshold values based upon the maximum and minimum monthly MODIS vegetation index for each land cover type to define the growing seasons. Let $T(l)$ be the threshold of land cover l. Any monthly grid point index larger than the biome-specific $T(l)$ indicates the grid point for that month is part of the growing season. As shown in Figure 2, the evergreen broadleaf forest has high indices throughout the year. Its growing season is set to 12 months and starts in January. For all other land cover types, we define the threshold itself as:

$$T(l) = (X_{\max}(l,m) - X_{\min}(l,m))/10 + X_{\min}(l,m) \qquad (3)$$

[19] It should be noted that in northern hemisphere, snow coverage will affect the vegetation signals, especially the minimum LAI/NDVI during winter. This will lower the biome-average threshold and extend the length of the growing season, which is more common in high-latitude forests. According to Yang et al. (submitted manuscript, 2004), about 30% of the high-latitude LAI (> 40°N) is affected by this snow effect during the winter. In order to alleviate the effects of snow, we have modified our methodology so that we only use the minimum LAI from nonsnow cover periods to calculate the growing season for high-latitude forests.

[20] Occasionally, the climatological LAI/NDVI profiles for a given pixel may show a bimodal curve, which indicates more than one growing season separated by months when the LAI/NDVI is smaller than the threshold. Figure 3 shows all pixels with more than one growing season. They are concentrated along the Eastern Africa coast, east China coast, and the Himalayas. The eastern China signals are highly affected by crop cycles, where double or triple cropping is common and the winter wheat is usually harvested around June [*Frolking et al.*, 2002]. This agrees with LAI signatures in which there is a decrease in June in all four years. Most continental pixels (97% from LAI; 96% from NDVI) have only one growing season. To make the later analysis easier, for the small fraction of pixels with more than one growing season, those with two growing seasons separated by only one month are joined into one growing season (to erase the effects from crop cycling). Otherwise, we chose the longer one or, if the growing season lengths are equal, we choose the one which includes the maximum growth month.

[21] Figure 4 shows the length of the growing season (i.e., the period for which the LAI/NDVI value is above the respective threshold for that biome type) and the start month of the growing season for each grid point (the month at which the LAI/NDVI value first goes above the threshold for that biome type). On a continental scale, Europe and South America have long growing seasons, up to 12 months, most of which start from November, December, or January. In Western Europe (mainly in France) some of the 12-month signal is due to the presence of evergreen forests. In addition, the croplands also have long growing seasons due to crop rotations. Winter crops such as winter rye are sown during late September or early October and germinate within a month [*Chmielewski*, 2003]. Although the anthesis of winter crops may start in spring at some regions, aerial biomass shows additional growth during the winter [*David et al.*, 2003], which will affect the satellite signals during this time and extends the growing season compared with similar biome regions. In contrast, north Africa has short growing seasons on average. In addition, from the Sahel to the central evergreen forests, the length of the growing season increases from one to 12 months, while the start of the growing season changes from August to January. Little or no vegetation activity is found in the Sahara desert, central southwest Asia (CSWA), center Australia, and Tibet.

[22] The NDVI and LAI estimates mainly agree with each other at continental scales. However, difference maps between the growing season lengths indicate that the NDVI tends to overestimate the growing season length in crop-

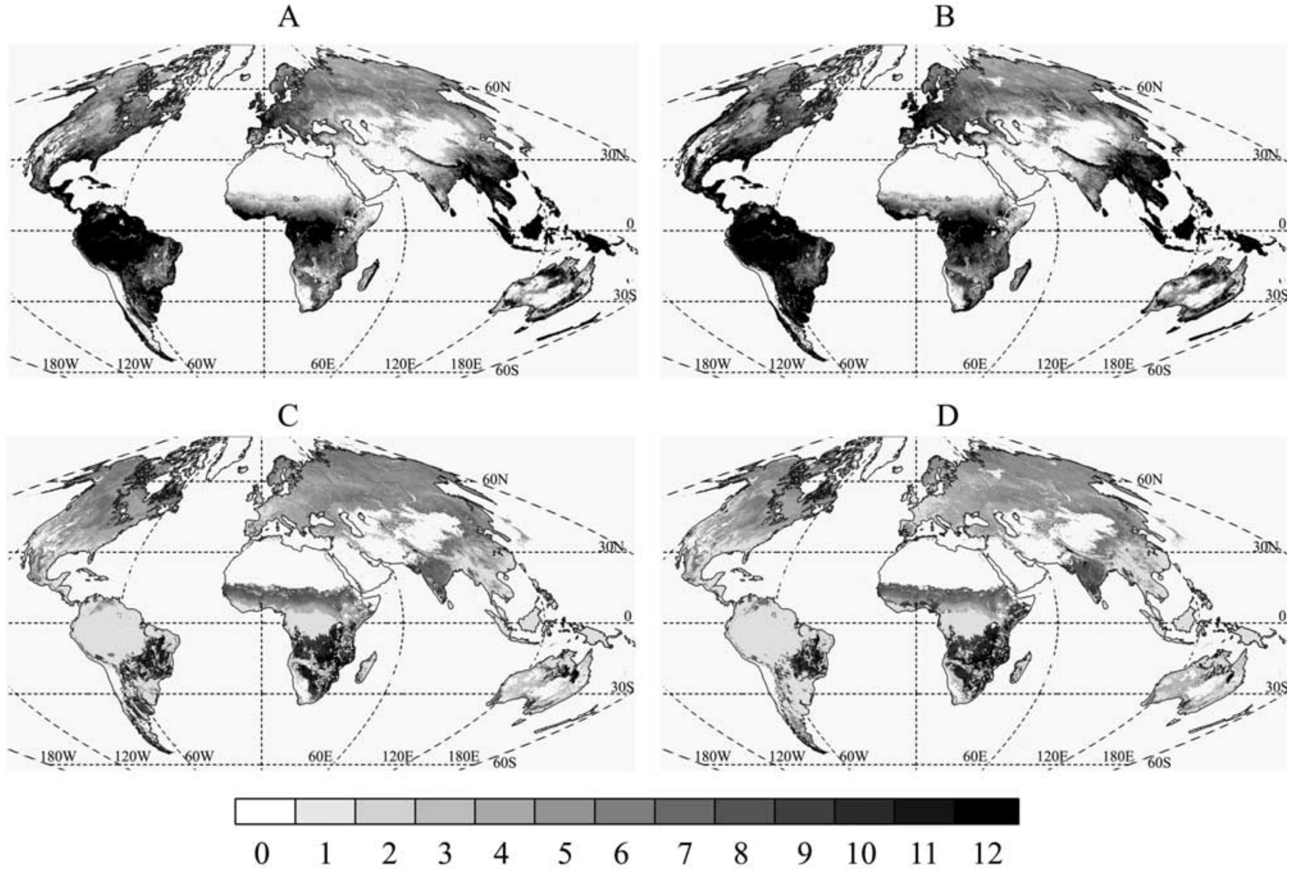

Figure 4. The length of the growing season in months and the start month of the growing season, generated from the MODIS products for each grid point at 16-km resolution. (a) Length of the growing season from MODIS LAI; (b) length of the growing season from MODIS NDVI; (c) start of the growing season from MODIS LAI; (d) start of the growing season from MODIS NDVI. See color version of this figure at back of this issue.

lands and forests (not shown). In addition, difference maps of the start month indicate these regions also show earlier start dates in the NDVI data (not shown). In general these regions correspond to those with long growing seasons, suggesting that the estimate of the growing season in these regions starts earlier and lasts longer when using the NDVI results. Both Figure 2 and previous studies [e.g., *Gitelson*, 2004] suggest that because NDVI approaches saturation asymptotically under conditions of moderate-to-high above-ground biomass, the saturation during the growing season will artificially lower the maximum value and hence the threshold in equation 3. As a result, the growing season estimated from NDVI extends longer and starts earlier. On the other hand, the larger variance in LAI can identify the variability during dense-growth periods and generate more accurate information on growing season.

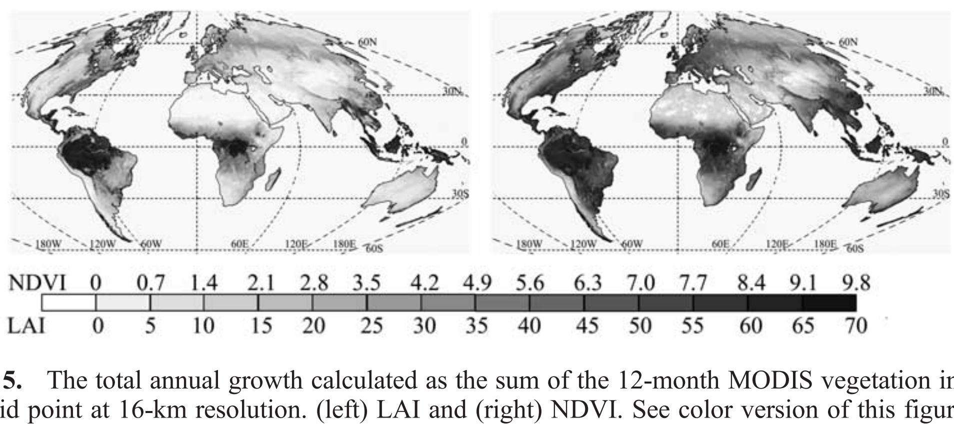

Figure 5. The total annual growth calculated as the sum of the 12-month MODIS vegetation index for each grid point at 16-km resolution. (left) LAI and (right) NDVI. See color version of this figure in the HTML.

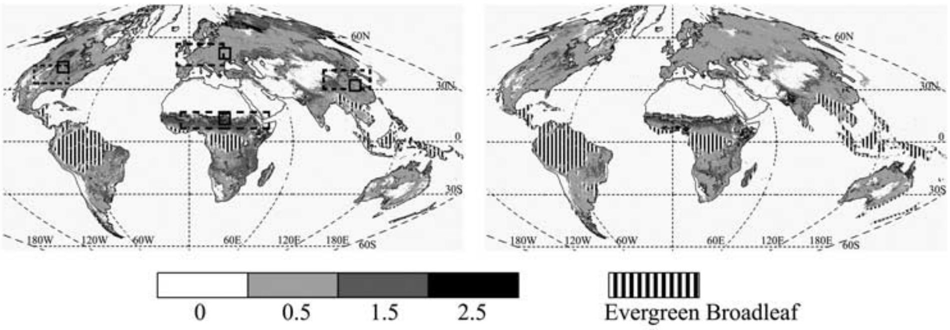

Figure 6. The climate impact index for each grid point at 16-km resolution (left) from LAI and (right) from NDVI. Solid boxes in Figure 6 (left) are sample regions chosen for Figure 7, and dashed boxes are sample regions chosen for Figure 10. See color version of this figure in the HTML.

[23] The annual vegetation growth is represented by the 12-month cumulative vegetation index (Figure 5). In both data products, evergreen broadleaf forests in South America and Africa have the maximum vegetation growth, while deserts in Sahara, CSWA, and Tibet have the minimum growth. The high latitudes in Asia have a north-south gradient of growth from 40N to 80N with a maximum growth band around 60N. From north Africa to south Africa, the growth increases from a minimum near the Sahara and reaches a maximum in the central forests, then descends back gradually again. Interestingly, the region between the Sahara desert and the central forest in Africa has an overall annual production similar to the west center of Europe, but the growing season in Africa is much shorter than the west center of Europe (see Figure 4); this result suggests that Africa has much higher productivity during its growing season and therefore may be more vulnerable to climatic variability during the peak growing months. This sensitivity will be quantified below.

[24] In general, though, at a continental and global scale, both the MODIS LAI and NDVI can identify the vegetation activity for different ecosystems. These MODIS products provide detailed information such as total annual production and actual growing season for any given location. However, the MODIS LAI has larger variability and can provide more specific information regarding the evolution and structure of the seasonal vegetation characteristics at a given grid point. On the other hand, the NDVI saturates around 0.7. It therefore tends to overestimate the growing season in regions where it is already long, especially those with croplands; in addition, it tends to overestimate the total growth in areas with minimal production, and to underestimate the growth in productive regions.

4. Characteristics and Evaluation of the Climatic Impact Index

[25] The previous section detailed the seasonal and annual growth for various regions based upon remotely sensed data from MODIS. This section examines how the relation between these values can provide additional information regarding the sensitivity of certain regions to potential changes in climatic variables. To do this, we derive a Climatic Impact Index (CII) for each pixel. For a given pixel p, let $M(p)$ be the length of the growing season and $M(l)$ be the average length of growing season for that land cover. The index $CII(p)$ is then calculated as

$$CII(p) = \frac{\sum_{m=1}^{12} X(p,m)/M(p)}{\sum_{m=1}^{12} X(l,m)/M(l)}. \tag{4}$$

[26] As a dimensionless number, the CII is the normalized growth rate in the growing season for each pixel, with the numerator representing the growth rate for that pixel and the denominator representing the average growth rate for its respective land cover type. By normalizing the growth rate with the biome-average growth rate, this index can identify the fractional amount of annual growth produced during the growing season, as opposed to the absolute amount which may be strongly weighted by the overall growth rate for different biome types. A CII around one indicates the growth rate of that pixel is similar to the average growth rate for its biome type. A CII larger than one suggests more than the biome-average growth is concentrated in the growing season. For these pixels, a one month loss of growth in the growing season will result in greater overall loss in the annual growth compared with pixels of similar biome type, suggesting grid points with higher CII values may be more vulnerable to climatic variability during the growing season. Because the time period of MODIS products is too short to generate a climatological profile, we are using the biome-type spatial average as a substitute for the grid point time average. As more temporal MODIS products become available in the future, it will be possible to use the grid point time average as opposed to the biome-type spatial average to calculate the CII (see below).

[27] Figure 6 shows the grid point CII values as derived from the LAI and NDVI data. Over most of the globe, the index is below 1.5, indicating average growth rates relative to the given biome types on a broad scale. However, there are interesting geographic variations. Europe and South America are the least sensitive continents. In contrast, regions surrounding the deserts in Sahara, CSWA, and Tibet tend to have extremely high CII values. Because NDVI values saturate at high productivity, the CII generated from NDVI generally shows smaller values when compared with those from LAI due to the fact that the growing season is

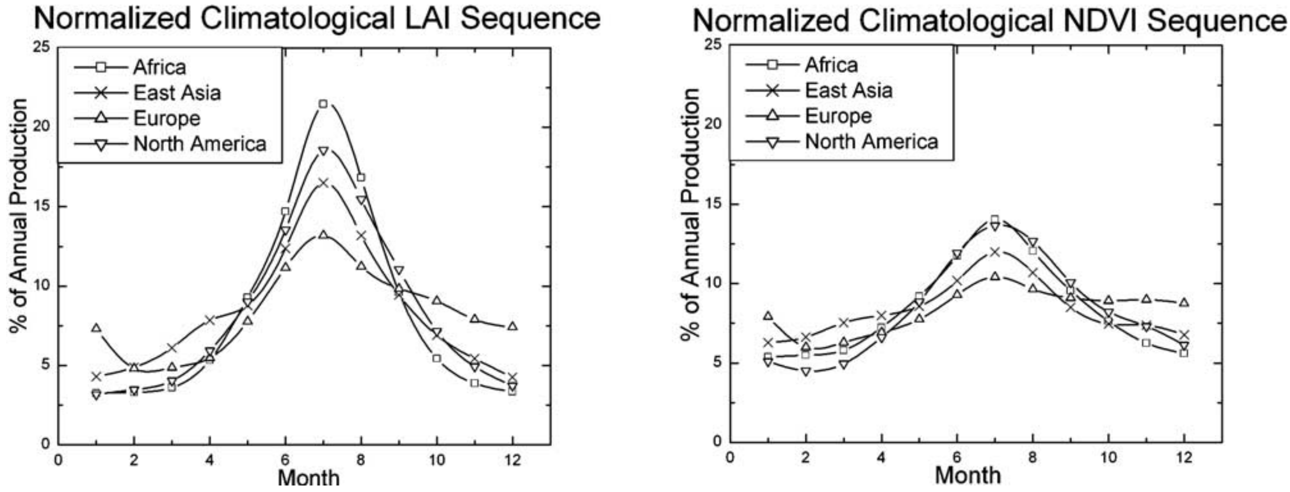

Figure 7. Normalized climatological sequence for 50 × 50 samples chosen from Africa, east Asia, Europe, and North America. Refer to the solid boxes in Figure 6 for the detailed locations. (left) LAI and (right) NDVI. The y axis is the percentage of the annual production. By shifting all the maximum growth months to July, the x axis represents the number of months (x - 7) apart from the maximum growth peak.

artificially longer and the total growth itself is artificially lower. Despite these differences, though, both products indicate that in the extremely sensitive regions like the Sahel, the total annual growth is highly concentrated in a relatively short growing season. In this case, 1 month loss of growth due to climatic variability during the growing season will result in a large overall loss in annual growth. In contrast, in the less sensitive regions like Europe, the total annual growth is evenly distributed in a longer growing season. One month loss of growth during the growing season in Europe may result in less loss in annual growth because of possible compensation in later months.

[28] These differences can be demonstrated by calculating the normalized spatial-average vegetation index for various regions (Figure 7). To eliminate the effect of timing of the growing seasons on the spatial average, we shifted the maximum growth months for each grid point to July, thereby centering the seasonal cycle upon July. We then calculated the area-average growth for each month. This allows us to focus on the average widths of the curves. If the area-average seasonal cycle is calculated according to the calendar year, the area-average curves in regions with strong spatial gradients in start dates tend to be artificially broader. Because of the shift in the seasonal cycle, the numbers along the x axis are no longer the real month, but instead indicate the number of months from the maximum growing peak. In addition, to better compare regions with different overall growth rates, the monthly vegetation indices (NDVI and LAI) are next normalized by the total annual production so that the y axis represents the fraction of the total annual growth.

[29] Samples are chosen from extremely sensitive regions like the Sahel, moderately sensitive regions like the United States and east China, and normal or nonsensitive regions like central Europe (solid boxes in Figure 6). All normalized spatial-average LAI/NDVI follow Gaussian distributions. However, Africa is represented by the curve with the largest amplitude and the smallest width, producing a narrow, peaked evolution. Europe's curve has the smallest amplitude and the broadest width. From the LAI curve, it can be seen that a 1-month loss of growth during the peak of the growing season would result in more than a 20% loss in the overall annual growth in Africa while resulting in less than a 15% loss in the overall annual growth in Europe; for longer climatic failures, two consecutive months of lost growth during the growing season would produce approximately a 35%–40% loss in the overall annual growth in Africa while producing only a 20%–25% loss in Europe. Although the results of NDVI have similar sequences as those of LAI, the variations of NDVI are much smaller because of the saturation. Overall, we see here that the CII metric, which isolates regions with intense growth over short periods, can effectively highlight those regions which may be more vulnerable to climatic variability during the growing seasons, when variability will have a larger impact upon total growth than during other times of year.

[30] To see whether the CII is related to interannual LAI variability at given locations, we use long time series GIMMS LAI as a substitute for MODIS LAI and compare the grid point CII values with the underlying variance of annual and growing season vegetation activity (Figure 8). In general, for both the annual LAI and the growing season LAI, the larger the variance in vegetation growth, the higher the CII is. In addition, regions in Africa, on average, have the largest CII and LAI variance, in agreement with the maps shown earlier. However, the relationship between CII and interannual variance is not one to one. For instance, grid points with the same variance in annual (or growing season) LAI can have very different CII values. However, even in these cases, the CII can provide an additional level of information by targeting those regions in which the vegetation variability is highly concentrated within a short set of growing season months and therefore may be more closely tied to climate variability over a particular time period.

5. Summary and Discussion

5.1. Summary

[31] The MODIS NDVI and LAI can quantify spatial differences between productivity of ecosystems as well as seasonal variations within ecosystems. By examining the

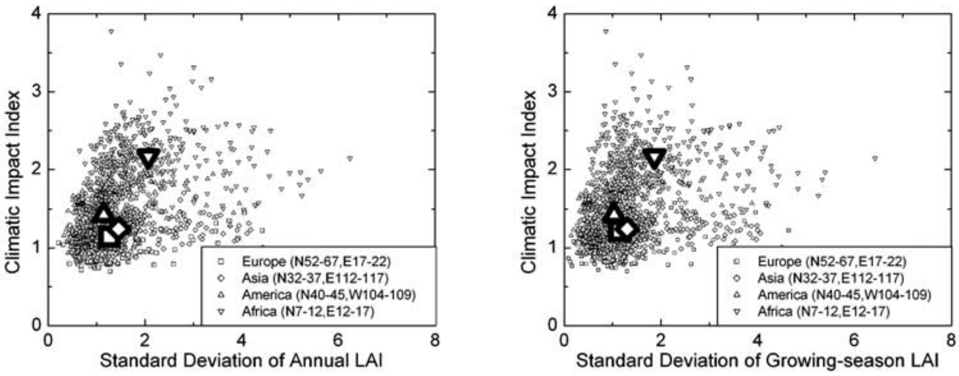

Figure 8. Correlation between CII and standard deviation of GIMMS LAI: (left) annual LAI and (right) growing season LAI. Nonforest vegetation samples are chosen from Africa (7°–12°N, 12°–17°E), east Asia (32°–37°N, 112°–117°E), Europe (52°–67°N, 17°–22°E), and North America (40°–45°N, 104°–109°W). CII are calculated from long time series average of GIMMS LAI (from 1982 to 2002). The corresponding symbol with black edge is the sample average for each region. See color version of this figure at back of this issue.

growing season and annual production, MODIS vegetation indices can provide detailed information on vegetation activity globally. At continental scales, the MODIS NDVI and LAI agree with each other with regard to growing season characteristics: Europe and South America have long growing season, up to 12 months; north Africa has a much shorter growing season. However, the LAI has better quality than the NDVI data, especially for high-growth regions. The saturation of NDVI in these regions artificially lowerers the threshold resulting in an overestimation of the growing season length and an earlier start date.

[32] Using derived characteristics of intraseasonal vegetation activity, a Climatic Impact Index is generated from the MODIS NDVI and LAI, which identifies regions like the Sahel that are sensitive to climatic change during the growing season such as droughts. Defined as the normalized growth rate in the growing season, the higher the CII, the larger the fraction of annual production that is concentrated in a growing season month, which indicates that in these regions overall annual growth is more sensitive to climatic variability during these short but high-growth periods. This sensitivity of the overall annual growth to climate variability during the growing season is captured by global maps of CII presented here. In addition, this sensitivity can be seen in the normalized spatial average values of MODIS LAI, which indicate that Africa can lose over 20% of the overall annual growth from a single 1-month loss of growth during the peak of the growing season. In contrast, Europe loses less than 15% of its annual growth from a 1-month loss during the peak growing season. Similar results are found when using NDVI as the basis for the CII, however because NDVI values saturate at high productivity, the CII generated from NDVI tends to underestimate the intraseasonal and interannual variability and hence the vegetation sensitivity.

[33] Because of the limited availability of the MODIS products, only 4 years of LAI could be used in this study so only the spatial attributes of CII are addressed in this paper. These limitations can be eliminated once more temporal MODIS LAI becomes available in the future. As an example, we use coarse resolution GIMMS LAI as a substitute of MODIS LAI and find that the CII in fact does provide information about the interannual variance in the vegetation growth for the underlying grid point. Below we discuss additional utility of the CII given longer time series data.

5.2. Discussion

[34] In this paper, a quantitative index was introduced to identify those regions that are particularly susceptible to vegetation loss due to climatic variability during the growing season. In addition to its use as a diagnostic tool, given the high spatial and temporal resolutions, this index can also be used for real-time monitoring, yield estimations, and climatic impact diagnosis. To see how the CII can be used for agricultural monitoring, we used AVHRR Pathfinder LAI to generate a long series of the CII. For a given pixel p, let $A(p)$ be the climatological annual LAI at month m and $T(p)$ be the climatologically annual LAI, then the index $CII(p, m, y)$ at month m year y is calculated as:

$$CII(p,m,y) = 100 \times \frac{X(p,m,y) - M(p,m)}{A(p)} \tag{5}$$

[35] In this formulation, the CII quantifies the percentage of the climatological annual grid point production either gained or lost due to climatic variability in one month. Figure 9 shows that the CII can capture historic drought events, such as the severe drought in Africa in 1984, which started in southern Africa and lasted through August, resulting in the lowest rainfall in 40 years in some areas [*LeComte*, 1985]; the national drought in United States in 1988, which was the result of a dry winter in 1987–1988 followed by a dry spring and produced decreased yields in certain areas of over 30% [*Heim*, 1988; *Johnson et al.*, 1993; *Kogan*, 1995]; and the global drought in 2000, which brought drought to North and East Africa, the Middle East, central Asia, and parts of North America [*LeComte*, 2001]. During these serious drought years, variations in the Climatic Impact Index indicate that there was a loss of up to

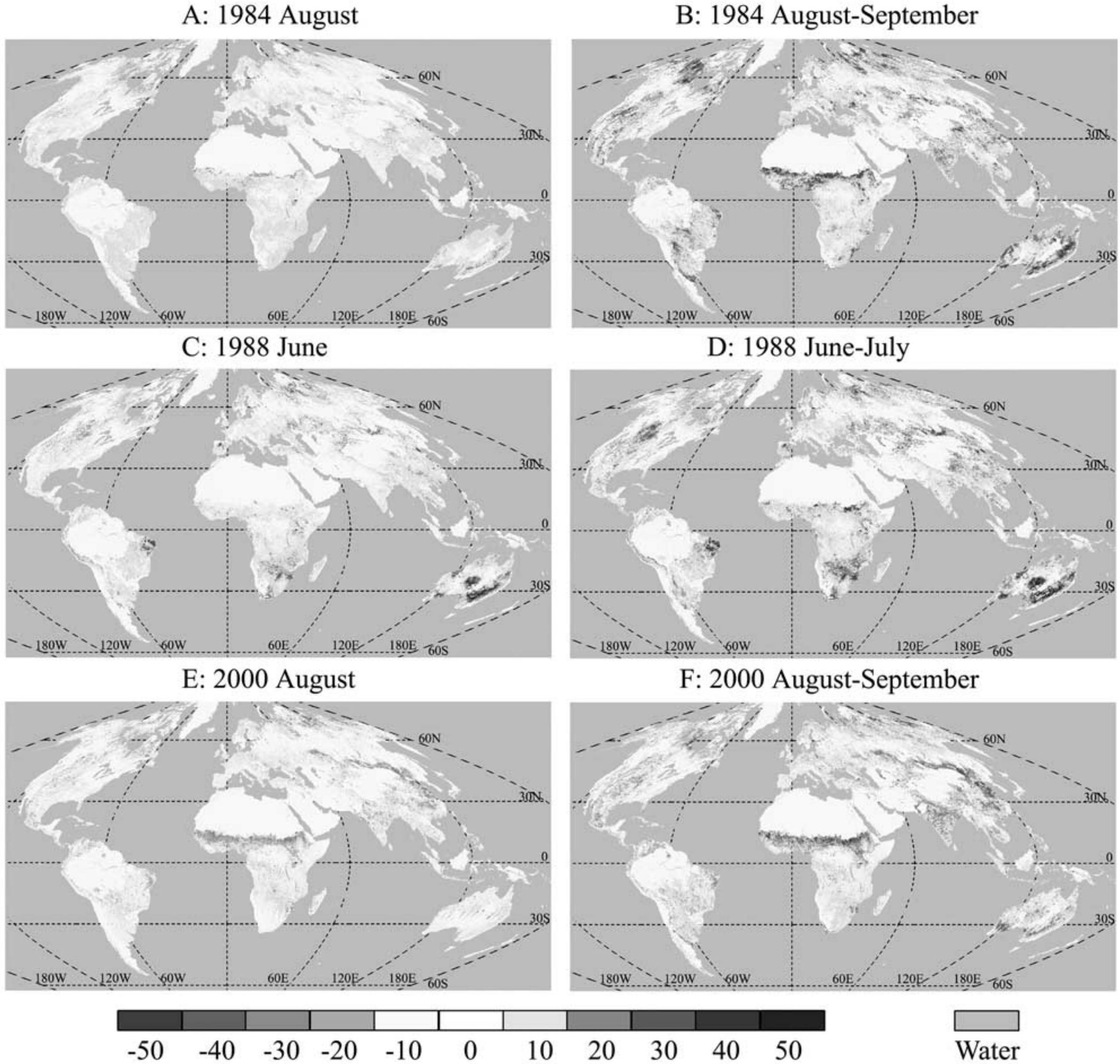

Figure 9. The temporal climatic impact index, representing the fraction of climatological annual production either gained or lost for each pixel at a 16-km resolution. (a) August 1984. (b) August and September 1984. (c) June 1988. (d) June and July 1988. (e) August 2000. (f) August and September 2000. The climatological annual production is averaged over the AVHRR Pathfinder LAI from 1982 to 2000. See color version of this figure at back of this issue.

50% of the total annual production in the impacted regions. Furthermore, the CII can also identify regions with an actual surplus of vegetation growth. For instance, during 1984, although the southern portion of the Sahel suffered severe decreases in vegetation growth, the region just to the south had large increases in growth, which could feasibly supply food to adjacent drought-stricken regions. Defined as the percentage of the annual production, then, the Climatic Impact Index can be used in real-time to estimate overall crop loss/gain during a particular month and may serve as a famine mitigation tool.

[36] To further investigate how the CII can serve as a possible indicator of climate-induced food loss, the Standardized Precipitation Index (SPI) is used to quantify the relationship between vegetation production and climate variables. The SPI is calculated from the monthly CMAP precipitation data from 1981 to 2000 at each grid point [*McKee et al.*, 1993]. Previous studies demonstrate that the ecosystems in arid and semiarid climate regimes are sensitive to seasonal precipitation anomalies [*Nicholson et al.*, 1990; *Lotsch et al.*, 2003]. In this paper, the 6-month SPI is used for the subsequent analysis. For each grid point (which is at $2.5^\circ \times 2.5^\circ$ resolution) the SPI anomaly is estimated. The corresponding LAI value $L(p, m, y)$ is found by averaging all the LAI pixels whose locations are within the SPI grid cell.

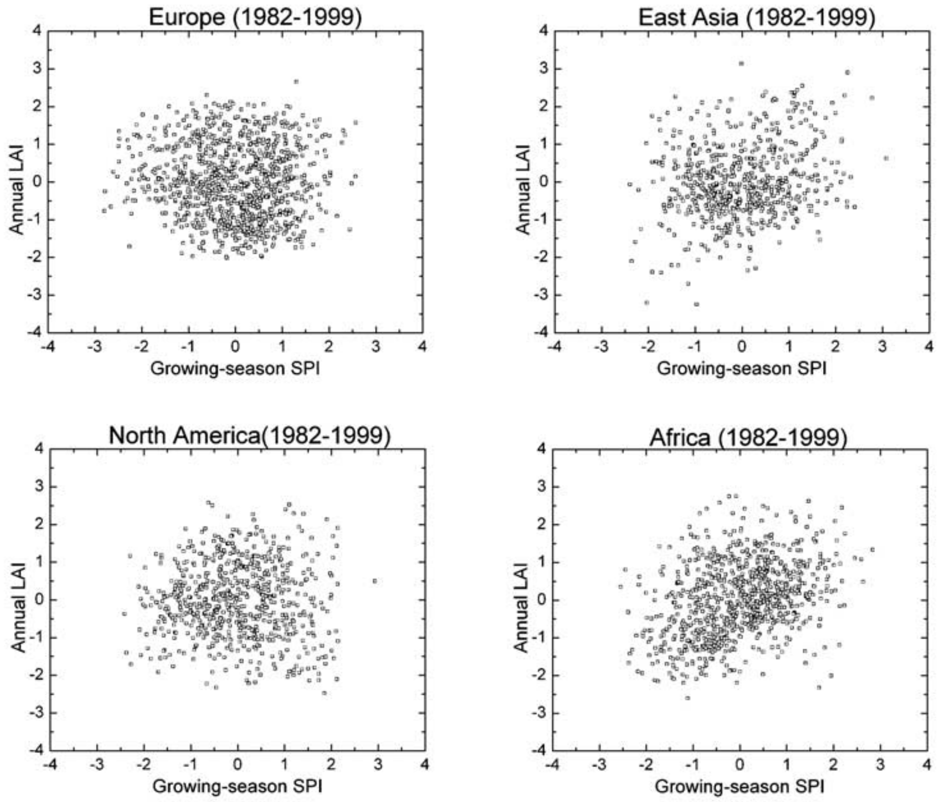

Figure 10. The relationship between annual Pathfinder LAI and growing season standardized precipitation index (SPI) for sample regions from Europe, east Asia, North America, and Africa. Refer to the dashed boxes in Figure 6 for the detailed locations. The 6-month SPI are computed from the CMAP data. Both the annual LAI and growing season SPI are standardized with respect to the individual grid point (see equation (6) for details).

[37] For each sample, the standardized anomaly of annual LAI is defined by

$$L'(p,y) = \frac{\sum_{m=1}^{12} L(p,m,y) - M(p)}{\sigma(p)}, \tag{6}$$

where M(p) is the mean of the annual LAI of the grid point *p*, and σ(p) is the standard deviation of the annual LAI of that point. The standardized anomaly of growing season SPI is similar except that the summation of the precipitation only accounts for months in the growing season. The relation between the standardized anomaly Pathfinder LAI and SPI provides an estimate of the proportion of annual vegetation production as a function of rainfall variability during the growing season.

[38] While vegetation indices and precipitation do have moderately high correlations in some areas, the relationship has a considerable degree of spatial heterogeneity [*Schultz and Halpert*, 1993; *Lotsch et al.*, 2003]. This may be seen in Figure 10, where relationships are very difficult to discern between the standardized annual Pathfinder LAI and growing season SPI in north Africa, east Asia, north America, and Europe (see the dashed boxes in Figure 6). It should be emphasized that similar results are found between the annual Pathfinder/GIMMS LAI and growing season CMAP, between the annual Pathfinder/GIMMS NDVI and growing season CMAP, and between annual Pathfinder/GIMMS NDVI and growing season SPI (not shown). Hence, although the annual vegetation production might climatologically be correlated with the climate variables (for example regions with more precipitation tend to grow more), our results demonstrate that there is no globally applicable correlation between vegetation indices (NDVI/LAI) and precipitation. This further highlights the need for consideration of both vegetation changes, as captured by CII, and precipitation deficits when monitoring drought impacts (as well as for further study of the varying relationships between the two across district level to multinational scales).

[39] It should be noted, however, that this CII is not the only possible remotely sensed monitoring tool. As mentioned in the introduction, Kogan's Vegetation Condition Index is widely used in the United States for drought monitoring and yield prediction. To evaluate the utility of the Climatic Impact Index introduced here, we calculate the VCI and CII at each grid point of the study regions and plot them against one another (Figure 11). Both the linear and polynomial functions show strong positive correlation between long time series of CII and VCI, which suggests that the CII and VCI provide similar information on vegetation production monitoring. It is interesting to note, however, that at the extremes of the VCI (both minimum

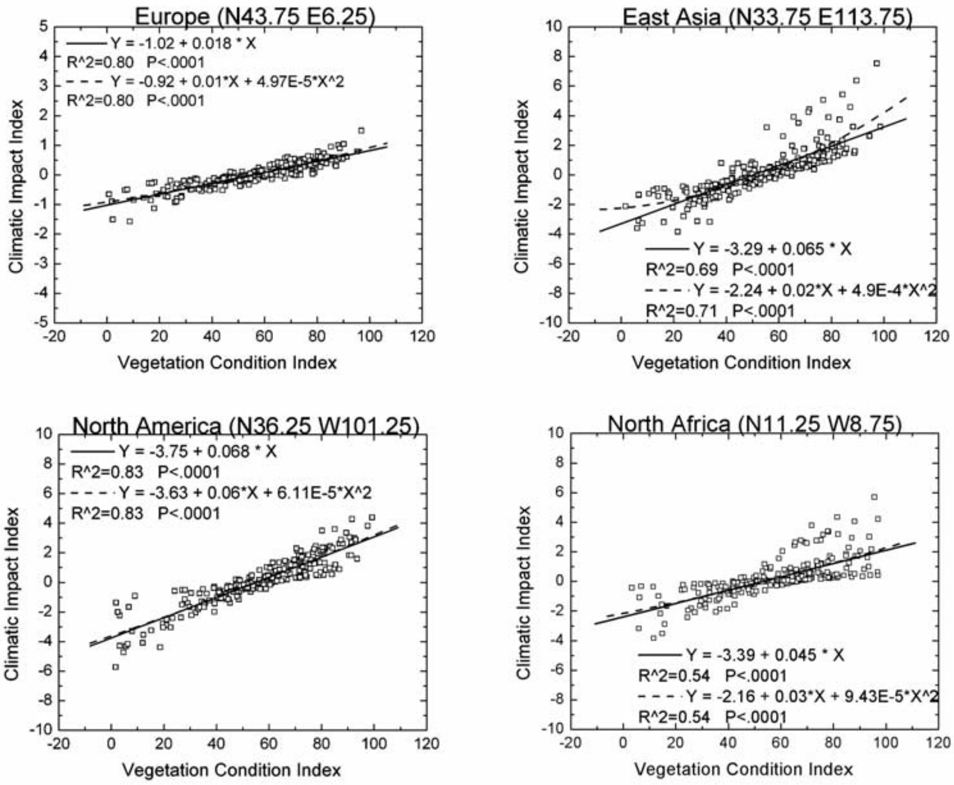

Figure 11. The correlation between the vegetation condition index (VCI) and climatic impact index (CII) for sample pixels from Europe, east Asia, North America, and Africa. The VCI is generated from monthly GIMMS NDVI from 1982 to 2001 at 0.25° resolution. The CII is generated from monthly GIMMS LAI from 1982 to 2001 at 0.25° resolution. Each sample is a 10 by 10 pixel average centered in each location. Both the linear and polynomial functions are shown in the plots.

and maximum), it appears that there are broad ranges in the CII, suggesting that at these extreme values, the CII adds information regarding the state of the vegetation not necessarily provided by the VCI alone. However, it is yet to be determined whether this result serves a practical purpose in monitoring itself; such impact studies are the subject of future research.

[40] **Acknowledgments.** We thank K. Didan and A. R. Huete at University of Arizona for providing the MODIS NDVI data set, and C. J. Tucker at NASA for providing the AVHRR GIMMS NDVI data. We also acknowledge X. Song and W. Yang at Boston University for the MODIS and AVHRR LAI data sets and discussions. This work was funded by the NASA Earth Science Enterprise under the MODIS contract to Boston University.

References

Carlson, T. N., and D. A. Ripley (1997), On the relation between NDVI, fractional vegetation cover, and leaf area index, *Remote Sens. Environ.*, *62*, 241–252.

Chmielewski, F.-M. (2003), Phenology and agriculture, in *Phenology: An Integrative Environmental Science*, edited by M. D. Schwartz, Kluwer Acad., Norwell, Mass.

David, C., M. H. Jeuffrony, S. Recous, and F. Dorsainvil (2003), Adaptation and assessment of the Azodyn model for managing the nitrogen fertilization of organic winter wheat, *Eur. J. Agron*, doi:10.1016/j.eja.2003.09.003.

Friedl, M. A., D. K. McIver, J. C. F. Hodges, X. Y. Zhang, D. Muchoney, A. H. Strahler, C. E. Woodcock, S. Gopal, A. Schneider, and A. Cooper (2002), Global land cover mapping from MODIS: Algorithms and early results, *Remote Sens. Environ.*, *83*, 287–302.

Frolking, S., J. Qiu, S. Boles, X. Xiao, J. Liu, Y. Zhuang, C. Li, and X. Qin (2002), Combining remote sensing and ground census data to develop new maps of the distribution of rice agriculture in China, *Global Biogeochem. Cycles*, *16*(4), 1091, doi:10.1029/2001GB001425.

Gitelson, A. A. (2004), Wide dynamic range vegetation index for remote quantification of biophysical characteristics of vegetation, *J. Plant Physiol.*, *161*(2), 165–173.

Goward, S. N., B. Markham, D. G. Dye, W. Dulaney, and A. J. Yang (1991), Normalized difference vegetation index measurements from the advanced very high resolution radiometer, *Remote Sens. Environ.*, *35*, 257–277.

Guttman, N. B. (1991), A sensitivity analysis of the Palmer hydrologic drought index, *Water Resour. Bull.*, *27*, 797–807.

Guttman, N. B. (1997), Comparing the Palmer drought index and the standardized precipitation index, *J. Am. Water Resour. Assoc.*, *34*, 113–121.

Guttman, N. B., J. R. Wallis, and J. R. M. Hosking (1992), Spatial comparability of the Palmer drought severity index, *Water Resour. Bull.*, *28*, 1111–1119.

Hayes, M., M. D. Svoboda, D. A. Wilhite, and O. V. Vanyarkho (1999), Monitoring the 1996 drought using the SPI, *Bull. Am. Meteorol. Soc.*, *80*, 429–438.

Heim, R. R., Jr. (1988), About that drought, *Weatherwise*, *41*(5), 266–271.

Heim, R. R., Jr. (2002), A review of twentieth-century drought indices used in the United States, *Bull. Am. Meteorol. Soc.*, *83*, 1149–1165.

Hu, Q., and G. D. Willson (2000), Effects of temperature anomalies on the Palmer drought severity index in the central United States, *Int. J. Climatol.*, *20*, 1899–1911.

Huete, A. R., C. Justice, and H. Liu (1994), Development of vegetation and soil indices for MODIS-EOS, *Remote Sens. Environ.*, *49*, 224–234.

Huete, A. R., H. Q. Liu, K. Batchily, and W. J. D. van Leeuwen (1997), A comparison of vegetation indices over a global set of TM images for EOS-MODIS, *Remote Sens. Environ.*, *59*, 440–451.

Johnson, G. E., V. R. Achutuni, S. Thiruvengadachari, and F. Kogan (1993), The role of NOAA satellite data in drought early warning and monitoring: selected case studies, in *Drought Assessment, Management, and Planning: Theory and Case Studies*, edited by D. A. Wilhite, pp. 31–49, Kluwer Acad., Norwell, Mass.

Justice, D. H., et al. (1998), The Moderate Resolution Imaging Spectroradiometer (MODIS): Land remote sensing for global change research, *IEEE Trans. Geosci. Remote Sens.*, *36*, 1228–1249.

Kogan, F. N. (1990), Remote sensing of weather impacts on vegetation, *Int. J. Remote Sens.*, *6*, 1417–1434.

Kogan, F. N. (1995), Droughts of the late 1980s in the United States as derived from NOAA polar-orbiting satellite data, *Bull. Am. Meteorol. Soc.*, *76*, 655–668.

LeComte, D. (1985), The year of the African drought, *Weatherwise*, *38*(1), 8–15.

LeComte, D. (2001), Weather around the world: In 2000, La Niña's impact was felt worldwide, *Weatherwise*, *54*(2), 23–27.

Lieth, H. (1970), Phenology in productivity studies, in *Analysis of Temperate Forest Ecosystems*, edited by D. E. Reichle, pp. 29–46, Springer-Verlag, New York.

Los, S. O. (1998), Estimation of the ratio of sensor degradation between NOAA AVHRR channel 1 and 2 from monthly NDVI composites, *IEEE Trans. Geosci. Remote Sens.*, *36*, 202–213.

Lotsch, A., M. A. Friedl, and B. T. Anderson (2003), Coupled vegetation-precipitation variability observed from satellite and climate records, *Geophys. Res. Lett.*, *30*(14), 1774, doi:10.1029/2003GL017506.

McKee, T. B., N. J. Doesken, and J. Kleist (1993), The relationship of drought frequency and duration to time scales, paper presented at 8th Conference on Applied Climatology, Am. Meteorol. Soc., Boston, Mass.

Myneni, R. B., R. R. Nemani, and S. W. Running (1997), Estimation of global leaf area index and absorbed par using radiative transfer models, *IEEE Trans. Geosci. Remote Sens.*, *35*, 1380–1393.

Myneni, R. B., et al. (2002), Global products of vegetation leaf area and fraction absorbed PAR from year one of MODIS data, *Remote Sens. Environ.*, *83*, 214–231.

Nicholson, S. E., M. L. Davenport, and A. R. Malo (1990), A comparison of the vegetation response to rainfall in the Sahel and East Africa, using normalized difference vegetation index from NOAA AVHRR, *Clim. Change*, *17*, 209–241.

Palmer, W. C. (1965), Meteorological drought, *Res. Pap. 45*, 58 pp., Weather Bur., U.S. Dep. of Commer., Washington, D. C.

Paltridge, G., and J. Barber (1988), Monitoring grassland dryness and fire potential in Australia with NOAA/AVHRR data, *Remote Sens. Environ.*, *28*, 384–393.

Peters, A. J., E. A. Walter-Shea, L. Ji, A. Viña, M. Hayes, and M. D. Svoboda (2002), Drought monitoring with NDVI-based standardized vegetation index, *Photogramm. Eng. Remote Sens.*, *68*(1), 71–75.

Reed, B. C., J. F. Brown, D. VanderZee, T. L. Loveland, J. W. Merchant, and D. O. Ohlen (1994), Measuring phenological variability from satellite imagery, *J. Vegetation Sci.*, *5*, 703–714.

Rosborough, G. W., D. G. Baldwin, and W. J. Enery (1994), Precise AVHRR image navigation, *IEEE Trans Geosci. Remote Sens.*, *32*, 644–657.

Running, S. W., et al. (1994), Terrestrial remote sensing science and algorithms planned for EOS/MODIS, *Int. J. Remote Sens.*, *15*, 3587–3620.

Schultz, P., and M. S. Halpert (1993), Global correlation of temperature, NDVI and precipitation, *Adv. Space Res.*, *13*, 277–280.

Sellers, P. J., S. O. Los, C. J. Tucker, C. O. Justice, D. A. Dazlich, G. J. Collatz, and D. A. Randall (1994), A global 1° by1° NDVI data set for climate studies. Part 2: The generation of global fields of terrestrial biophysical parameters from the NDVI, *Int. J. Remote Sens.*, *15*, 3519–3545.

Sellers, P. J., et al. (1997), Modeling the exchanges of energy, water, and carbon between continents and the atmosphere, *Science*, *275*, 502–509.

Tian, Y., et al. (2004), Comparison of seasonal and spatial variations of LAI/FPAR from MODIS and Common Land Model, *J. Geophys.*, 109, D01103, doi:10.1029/2003JD003777.

Vermote, E. F., and Y. J. Kaufman (1995), Absolute calibration of AVHRR visible and near-infrared channels using ocean and cloud views, *Int. J. Remote Sens.*, *16*, 2317–2340.

Vermote, E., N. El Saleous, Y. J. Kaufman, and E. Dutton (1997), Data pre-processing: Stratospheric aerosol perturbing effect on the remote sensing of vegetation: Correction method for the composite NDVI after the Pinatubo eruption, *Remote Sens. Rev.*, *15*, 7–21.

Vermote, E., N. El Saleous, and C. Justice (2002), Atmospheric correction of the MODIS data in the visible to middle infrared: First results, *Remote Sens. Environ.*, *83*, 97–111.

Waggoner, P. E. (1974), Modeling seasonality, in *Phenology and Seasonality Modeling*, edited by H. Lieth, pp. 301–322, Springer-Verlag, New York.

White, M. A., P. E. Thornton, and S. W. Running (1997), A continental phenology model for monitoring vegetation responses to interannual climatic variability, *Global Biogeochem. Cycles*, *11*, 217–234.

Wilhite, D. A., and M. A. Glantz (1985), Understanding the drought phenomenon: The role of definitions, *Water Int.*, *10*, 111–120.

Xie, P., and P. A. Arkin (1997), Global precipitation: A 17-year monthly analysis based on gauge observations, satellite estimates and numerical model outputs, *Bull. Am. Meteorol. Soc.*, *78*, 2539–2558.

Zhang, X., M. A. Friedl, C. B. Schaaf, A. H. Strahler, J. C. F. Hodges, F. Gao, B. C. Reed, and A. Huete (2003), Monitoring vegetation phenology using MODIS, *Remote Sens. Environ.*, *84*, 471–475.

B. Anderson, R. B. Myneni, B. Tan, and P. Zhang, Department of Geography, Boston University, 675 Commonwealth Avenue, Boston, MA 02215, USA. (zhping@crsa.bu.edu)

M. Barlow, Atmospheric and Oceanic Diagnostics, AER. Inc, Lexington, MA 02421, USA.

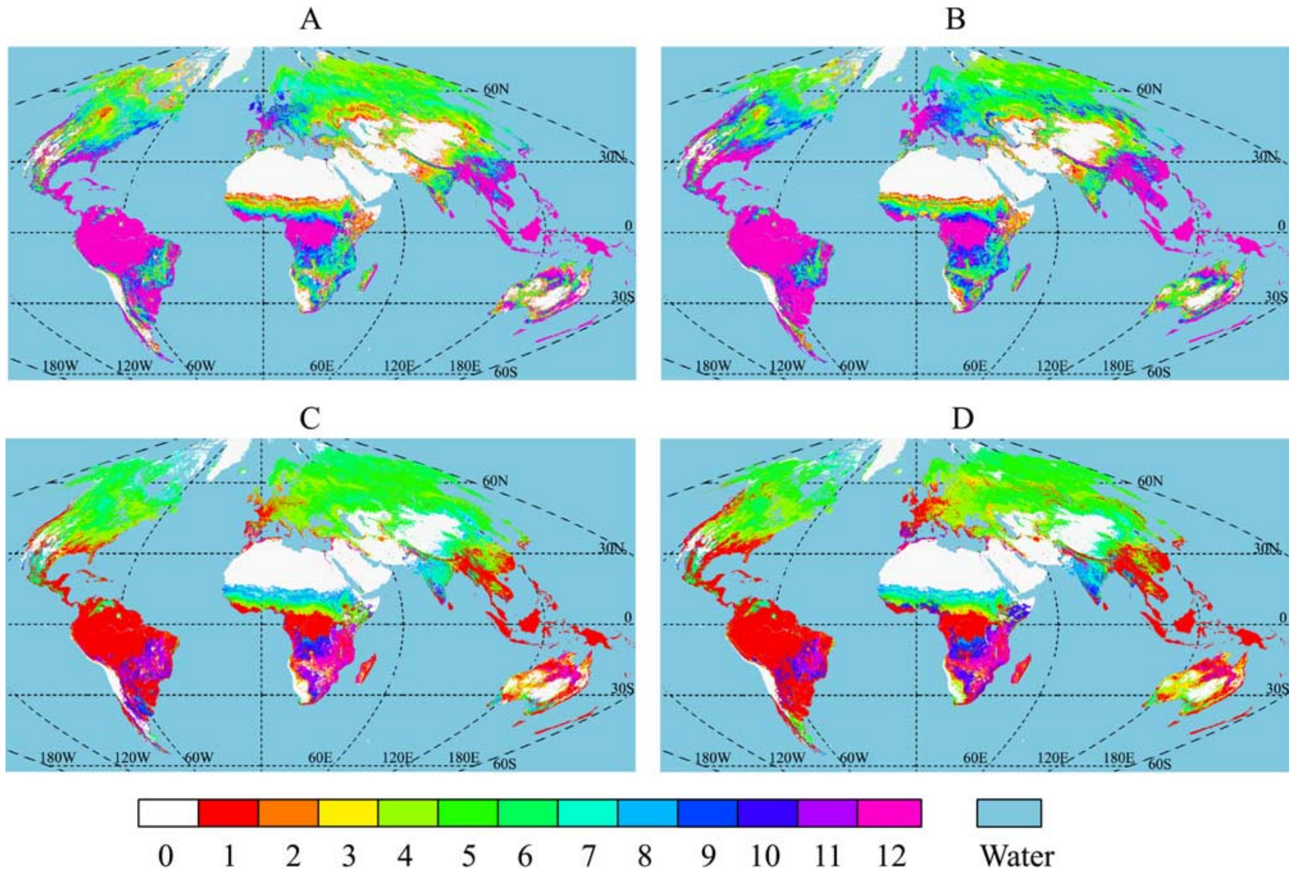

Figure 4. The length of the growing season in months and the start month of the growing season, generated from the MODIS products for each grid point at 16-km resolution. (a) Length of the growing season from MODIS LAI; (b) length of the growing season from MODIS NDVI; (c) start of the growing season from MODIS LAI; (d) start of the growing season from MODIS NDVI.

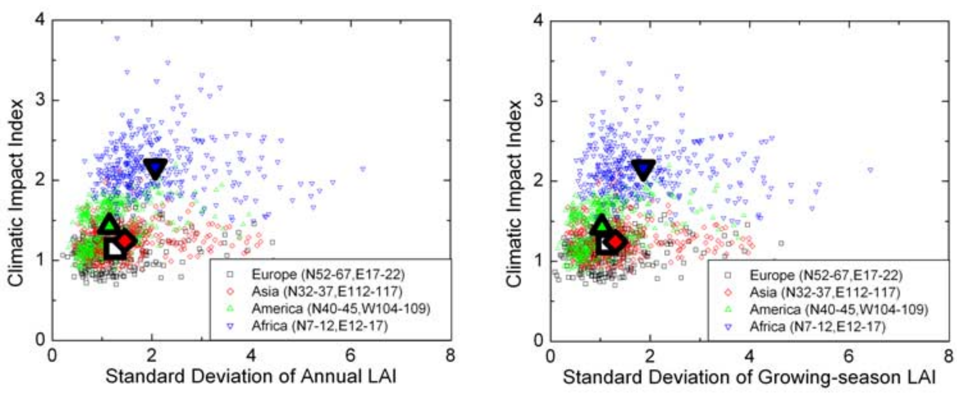

Figure 8. Correlation between CII and standard deviation of GIMMS LAI: (left) annual LAI and (right) growing season LAI. Nonforest vegetation samples are chosen from Africa (7°–12°N, 12°–17°E), east Asia (32°–37°N, 112°–117°E), Europe (52°–67°N, 17°–22°E), and North America (40°–45°N, 104°–109°W). CII are calculated from long time series average of GIMMS LAI (from 1982 to 2002). The corresponding symbol with black edge is the sample average for each region.

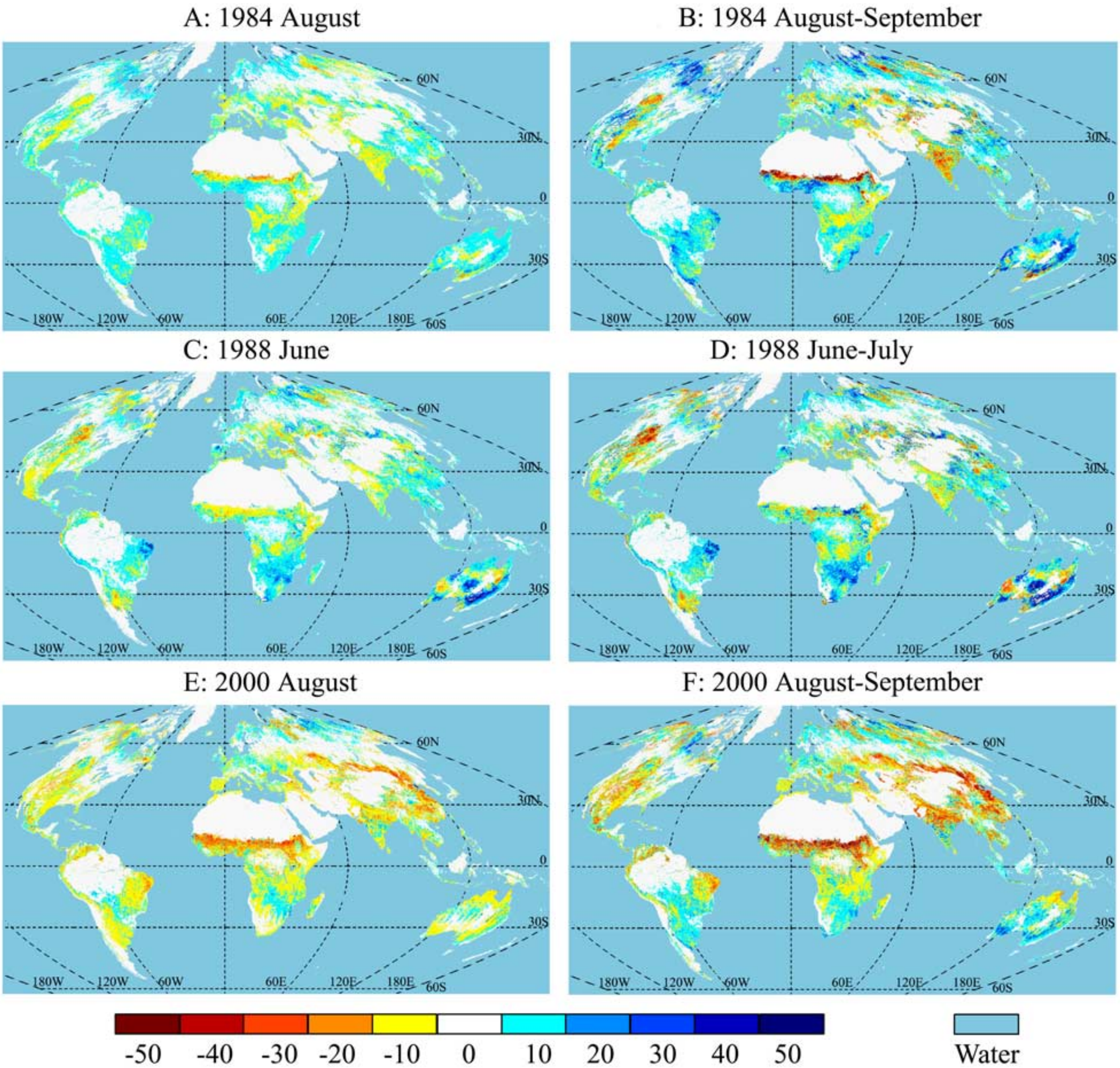

Figure 9. The temporal climatic impact index, representing the fraction of climatological annual production either gained or lost for each pixel at a 16-km resolution. (a) August 1984. (b) August and September 1984. (c) June 1988. (d) June and July 1988. (e) August 2000. (f) August and September 2000. The climatological annual production is averaged over the AVHRR Pathfinder LAI from 1982 to 2000.